

Shaper-assisted collinear SPIDER: fast and simple broadband pulse compression in nonlinear microscopy

Bernhard von Vacano, Tiago Buckup, and Marcus Motzkus

Physikalische Chemie, Philipps-Universität Marburg, Hans-Meerwein Strasse, D-35032 Marburg, Germany

Received October 25, 2006; accepted January 3, 2007;
posted January 25, 2007 (Doc. ID 76409); published April 17, 2007

In situ characterization and control of the phase of broadband femtosecond pulses in microscopy can be achieved with a novel simplified scheme based on spectral shear interferometry for direct electric field reconstruction (SPIDER): the use of a femtosecond pulse shaper eliminates the need for an interferometer setup, allows dispersion-free SPIDER operation and at the same time compression even of complex pulses. Beyond compression, the scheme allows precise phase control at the site of the microscopic experiment. We present the underlying principles, design considerations, and details of the experimental implementation, and show the successful operation of the shaper-assisted collinear (SAC) SPIDER to characterize, compress, and tailor broadband femtosecond pulses *in situ*. The reliability is demonstrated by comparison with independent cross-frequency-resolved optical gating measurement, and improved multiphoton imaging with SAC-SPIDER-compressed pulses is shown. Its simplicity and versatility make SAC-SPIDER an extremely useful tool for next-generation broadband nonlinear microscopy. © 2007 Optical Society of America

OCIS codes: 320.5520, 180.0180, 320.5540, 170.6900.

1. INTRODUCTION

In multiphoton microscopy, high excitation intensities are essential for the efficiency of nonlinear optical processes serving as contrast mechanisms. Intrinsicly, this allows high three-dimensional spatial resolution with the signal generation being confined to the focal volume.¹ On the technical side, pulsed laser sources usually have to be employed, with their very advantageous high peak intensities at low average powers, which is utterly desirable for non-destructive imaging. From this point of view, femtosecond lasers are ideally suited for multiphoton microscopy. However, the shorter femtosecond pulses are, and thus the more efficient a nonlinear excitation can be, the more they are susceptible to broadening in time due to the dispersion of optical elements, which introduce distortions in the spectral phase. In conventional femtosecond spectroscopy, dispersive optics are usually avoided for that reason whenever possible. In microscopy though, to realize the highest spatial resolution and imaging quality, elaborate microscope objectives are used, which consist of many dispersive elements. Therefore, to obtain high peak intensities with as short pulses as possible, inevitable distortions of the spectral phase have to be compensated for, for imaging under optimal conditions.² Furthermore, some femtosecond sources, for example, inexpensive and compact fiber-based femtosecond lasers, emit pulses with a spectral phase far from the Fourier-limit case. Only if this can also be accounted for in the compensation of spectral phase distortions, will such a nonlinear microscope reach its full potential.

Typically, the linear dispersion of femtosecond laser

pulses in microscopy has been compensated for by using grating- or prism-based passive compressor schemes,^{3–6} adjusting the compressor to maximize a nonlinear signal from the microscope focus. For even shorter femtosecond pulses, however, higher-order dispersion becomes increasingly important. Additionally, the adjustment of passive compressors is time consuming and the setup is rather inflexible. Very flexible compression of arbitrary phase distortions in the context of microscopy can be achieved by employing femtosecond pulse shaping, typically implemented in a $4f$ setup.⁷ This allows very rapid and flexible pulse compression, in particular under changing experimental conditions. However, to correct the phase distortions, the appropriate phase to be applied by the pulse shaper has to be found. A simple, yet rather slow approach is to use a nonlinear signal or an autocorrelation trace measured at the site of the microscopic sample as feedback in an optimization, which is typically based on a genetic algorithm learning loop.^{8–10}

A direct approach would be the *in situ* characterization of the femtosecond pulses, and thus the determination of their spectral phase, and applying this inverted phase as a correction in the shaper. There are several schemes that have been applied or have the potential for *in situ* pulse characterization in microscopy. These schemes are all based on collinear beam geometry, which is necessary for use with high numerical aperture microscope objectives. One possibility is collinear frequency-resolved optical gating (FROG), which has been demonstrated under the conditions of microscopy.^{11–13} However, the scanning of the temporal delay during the FROG measurement and nec-

essary iterative reconstruction after the acquisition of the data makes this technique rather slow and prevents a practical use for direct feedback of the retrieved phase for compression. There are other methods also relying on the subsequent scanning of a parameter to measure the spectral phase, which are already based on the presence of a pulse shaper in the experimental setup. One approach is time-domain nonlinear interferometry, where the necessary sequence of pulses with variable delay is generated by pulse shaping.¹⁴ From the obtained interferogram, the spectral phase of the input pulse can be extracted and used for compression. This scheme has not explicitly been demonstrated for microscopy, but should be directly applicable due to its single-beam nature. Another possible approach, equally relying on only a single beam, is the multiphoton intrapulse interference phase scans (MIIPS) technique.¹⁵ Here, the spectral phase of pulses is determined *in situ* by applying subsequently varying reference phase modulations, recording the frequency resolved second-harmonic spectrum, and iterating this correction several times until the phase compensation is sufficient. MIIPS has been demonstrated in microscopy.¹⁶

The techniques mentioned so far are relatively slow and require scanning of at least one parameter. Therefore, they are not capable of a real-time characterization of the spectral phase. This highly desirable capability, even for the measurement of very complex phases, is provided by spectral shear interferometry for direct electric field reconstruction (SPIDER).^{17–19} Consequently, we have recently developed a shaper-assisted collinear (SAC) SPIDER (SAC-SPIDER); a collinear implementation for use in microscopy.²⁰ This novel scheme greatly simplifies the experimental setup by the use of the pulse shaper, and allows precise and very rapid *in situ* total phase control. In this paper, we describe in detail the implementation and operation of SAC-SPIDER, discuss issues of calibration and reproducibility, compare the technique with an *in situ* implementation of the well-known cross-FROG, and demonstrate its great utility for nonlinear microscopy.

2. THEORY AND DESIGN CONSIDERATIONS

A. SPIDER Principle

Spectral interferometry techniques are based on the comparison of two mutually coherent beams. However, these techniques are only sensitive to the relative phase between the two sources. To measure the absolute phase of one of the beams, the phase of the other must be known beforehand. A way out of this tight requirement is to use a self-referencing modification of spectral interferometry, such as the SPIDER method.^{17–19} In the SPIDER method, the unknown test pulse is duplicated and both replicas are upconverted by mixing with a strong chirped reference pulse. The two upconverted replicas interfere and from the interferogram the spectral phase of the unknown pulse can be unambiguously retrieved. The self-referencing in the SPIDER method is achieved by delaying the two replicas against each other by a delay τ before the sum-frequency process. It ensures that each replica will mix with a different single frequency of the chirped reference pulse. The phase reconstruction in the SPIDER

method is a straightforward process known from interferometry²¹ and has been discussed in several publications in the context of SPIDER.^{17,18,22} Very briefly, the interferogram is initially Fourier transformed and one sideband in the time domain centered at delay τ is filtered out. The filter width was found to be not very critical and independent on the signal-to-noise ratio.²³ This sideband is then transformed back to the frequency domain with an inverse fast Fourier transform (FFT). That way, the phase variation of the unknown test pulse is obtained. The phase can then be directly reconstructed by a concatenation or integration process. The delay τ generates a linear term that can be easily measured in the experiment and needs to be subtracted as described in Section 3. If this term is not correctly determined, it will give rise to a quadratic contribution in the reconstructed phase, which cannot be distinguished from such phase terms of unknown pulses.

The phase variation in the frequency domain is sampled with a frequency step given by the spectral shear Ω . That means that the choice of the spectral shear Ω cannot be arbitrary: for Gaussian-shaped pulses, a ratio between the spectral width and the shear of approximately a factor of 4 is enough to reconstruct the phase correctly. Depending on the complexity of the spectra, however, the shear must be chosen to be ~ 20 – 25 times smaller than the spectral bandwidth.²³ On the other hand, the frequency shear Ω is dependent on the amount of delay τ between the replicas and of the group-delay dispersion (GDD) used to generate the chirp of the reference pulse:

$$\Omega = \frac{\tau}{\text{GDD}}. \quad (1)$$

In practice, the amount of delay τ is chosen such that the sideband after the FFT in the phase reconstruction procedure is well separated from the central peak, and that the number of fringes in the interferogram can still be resolved with the given spectrometer resolution. The Whittaker–Kotelnikov–Shannon sampling theorem states that in order to correctly sample the fringes, there must be at least two data points per fringe. The actual sampling rate required will be somewhat higher because of noise and other possible perturbations. It has been shown that a number of at least 20 fringes is enough to reconstruct the phase correctly.¹⁹ Thus, for a given optimal delay τ the spectral shear Ω is fixed. Additionally, the amount of GDD of the reference pulse has to ensure that the instantaneous frequency is approximately constant during the unknown test pulse duration. Of course, even with optimized Ω , τ , and GDD, the maximum relative phase variation that can be measured with spectral interferometry is still limited by the spectral resolution of the spectrometer.

The SPIDER method has, however, the disadvantage that the unknown pulse must be split in two delayed replicas, which adds dispersion. To avoid additional dispersion for the test pulse in an interferometer, a zero additional phase (ZAP) SPIDER has been proposed,²² where the chirped reference pulse is split into a doublet and mixed with an unmodified input pulse. The ZAP-SPIDER has the advantage that the delay between the upcon-

verted replicas is now independent on the frequency shear. Both can be adjusted separately. However, this modified scheme cannot be implemented in a collinear geometry and is more complex to realize experimentally. Very recently, variants of such a SPIDER scheme relying only on an unmodified input pulse have been demonstrated based on spatial²⁴ or collinear time-domain interferograms.²⁵

The choice of the nonlinear process for frequency conversion also plays an important role in the SPIDER method and its variants. In this sense, type-II phase-matched crystals are the best choice for the sum-frequency generation due to their larger phase-matchable bandwidth. Additionally, they are a prerequisite for background-free sum-frequency mixing in collinear beam geometry. It has to be mentioned that SPIDER methods, in general, tolerate even significant variations of the up-conversion efficiency across the pulse spectrum, because the information content of the SPIDER interferogram is within the fringe spacing, and not the amplitude. Therefore, a precise SPIDER measurement can still be performed in cases where the supported upconversion bandwidth is not sufficient for correlation-type measurements.²⁶

B. Basics of SAC-SPIDER

There is a possibility to construct a completely dispersion-free interferometer for the SPIDER setup: a pulse shaper, capable of phase and amplitude modulation, can be used to create double pulses, identical copies of the test pulse, which can then be upconverted by mixing with the chirped reference pulse. For experiments that rely on a shaper anyway (for pulse compression or coherent control^{27,28}), this means that there is no need to introduce any other element in the beam path. It is only necessary to program the shaper for SPIDER compression.²⁰ To create double pulses with a temporal separation τ , the desired pulse-shaping effect in the time domain is a convolution of the input pulse with two Dirac delta functions at $t + \tau/2$ and $t - \tau/2$ [Fig. 1(a)],

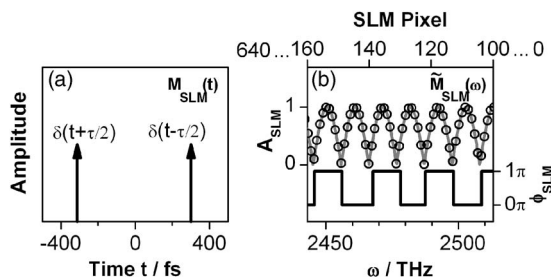


Fig. 1. Creation of double pulses with the femtosecond pulse shaper. (a) Shaping target $M_{SLM}(t)$ in the time domain for the generation of the desired identical copies of the input pulse with a separation $\tau=600$ fs in this case. (b) Corresponding frequency domain modulation $\tilde{M}_{SLM}(\omega)$ with amplitude $A_{SLM}(\omega)$ and phase $\varphi_{SLM}(\omega)$ as realized by the pixilated SLM in the Fourier plane of the $4f$ pulse shaper. For clarity, only a section of the 640 pixel range is shown. For the given case ($\tau=600$ fs), it can be seen that each period is rendered by 18 pixels, which is well above the Nyquist limit (see text).

$$E_{out}(t) = E_{in}(t) \otimes M_{SLM}(t) = \int_{-\infty}^{+\infty} d\tau E_{in}(\tau) \frac{1}{2} \left[\delta\left(t + \frac{\tau}{2}\right) + \delta\left(t - \frac{\tau}{2}\right) \right]. \quad (2)$$

To achieve such a shaping with a $4f$ pulse shaper,⁷ in the frequency domain the following mask function $\tilde{M}_{SLM}(\omega)$ has to be applied to the input spectrum [Eqs. (3) and (4)],

$$\tilde{E}_{out}(\omega) = \tilde{E}_{in}(\omega) \tilde{M}_{SLM}(\omega), \quad (3)$$

where $\tilde{M}_{SLM}(\omega)$ is given by

$$\begin{aligned} \tilde{M}_{SLM}(\omega) &= FT^{-1} \frac{1}{2} \left\{ \delta\left(t + \frac{\tau}{2}\right) + \delta\left(t - \frac{\tau}{2}\right) \right\} \\ &= \underbrace{abs \left[\cos\left(\frac{\omega\tau}{2}\right) \right]}_{\text{amplitude } A_{SLM}(\omega)} \exp \left\{ i \underbrace{\arg \left[\cos\left(\frac{\omega\tau}{2}\right) \right]}_{\text{phase } \varphi_{SLM}(\omega)} \right\}. \end{aligned} \quad (4)$$

For a liquid-crystal spatial light modulator (SLM), this mask function is rendered as a discrete pattern on the pixels [Fig. 1(b)] modulating the input spectrum in phase and amplitude. The modification of the period of the mask function in Eq. (4) (parameter τ) enables the delay between the two replicas to be easily adjusted. Additional phase shaping is possible simply by adding a correction phase $\varphi_{corr}(\omega)$ to $\varphi_{SLM}(\omega)$, leading to a modified mask function $\tilde{M}_{SLM}(\omega)$. The maximum achievable delay τ depends on the number N of pixels illuminated by the spectrum and is limited by the Whittaker–Kotelnikow–Shannon sampling theorem. To create a clean double pulse, each oscillation of the mask function $\tilde{M}_{SLM}(\omega)$ has to be rendered with at least four pixels to ensure that $\tilde{M}_{SLM}(\omega)$ is well defined. This case constitutes the Nyquist limit. Hence, one can approximate that

$$\tau < \frac{\pi N}{2\Delta\omega}, \quad (5)$$

where $\Delta\omega$ is the bandwidth transmitted through N pixels.

The second essential requirement of SAC-SPIDER is collinear sum-frequency mixing under tight focusing conditions. Such sum-frequency generation (SFG) using high numerical aperture objectives, however, is rather easily implemented and even shows advantages over more conventional optical setups: due to the tight-focusing condition, a much broader bandwidth can be phase matched and the effects of walk-off are strongly minimized.^{11,29}

3. EXPERIMENTAL IMPLEMENTATION

The experimental setup is depicted in Fig. 2. The primary laser source used in this study is a standard Ti:sapphire oscillator. It delivers 100 fs pulses with a central wavelength of 795 nm at 80 MHz repetition rate. Of this laser output, 25% are picked off³⁰ and a linear chirp ϕ'' of 37,000 fs² is introduced for SPIDER measurements by a grating stretcher. This provides the intense chirped reference beam for the generation of the spectrally sheared

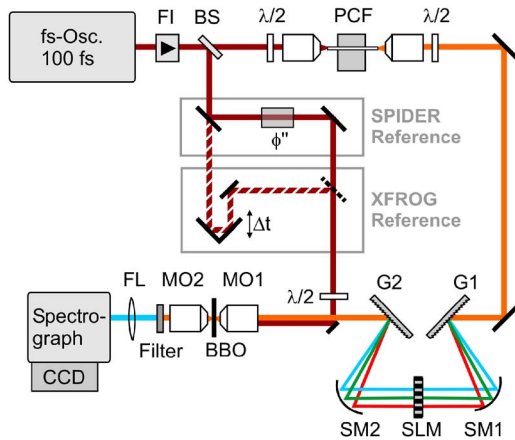


Fig. 2. (Color online) Experimental setup. The femtosecond oscillator output beam is sent through a Faraday isolator (FI) and then split into two parts. Seventy-five percent of the energy is used to generate supercontinuum in a PCF sent into the femtosecond pulse shaper (G1-2, gratings; SM1-2, spherical mirrors; SLM, spatial light modulator with 640 pixels for phase and amplitude modulation). The remaining 25% of oscillator energy is used to provide an orthogonally polarized reference beam, which is chirped (ϕ'') for the SPIDER measurement. Both beams are collinearly superimposed and focused (MO1-2, microscope objectives) into a type-II BBO crystal at the position of the sample. The SFG is finally analyzed in a spectrograph (FL, focusing lens). The hatched beam indicates an alternative path for *in situ* XFROG measurements, where the reference beam is not chirped, but delayed by a variable time Δt .

replica. The use of a grating stretcher is by no means necessary or ideal; the introduction of linear chirp can be accomplished much more easily with a simple rod of highly dispersive glass. Finally, the polarization of the reference beam is rotated 90° with a $\lambda/2$ wave plate. The broadband femtosecond pulses to be compressed in this work with SAC-SPIDER stem from nonlinear spectral broadening in a photonic crystal fiber (PCF). This supercontinuum is created by focusing the remaining fundamental laser beam (~ 3 nJ pulse energy) into a polarization maintaining PCF (Crystal Fibre, NL-PM 800, 24 mm). The resulting continuum with 1.2 nJ pulse energy is sent into a $4f$ pulse shaper, consisting of two gratings (1200 grooves/mm, G1-2) and two spherical mirrors ($f=200$ mm, SM1-2). In the Fourier plane, phase and amplitude of each spectral component can be modulated by a dual mask 640 pixel liquid-crystal SLM with parallel thin-film polarizers. The shaper configuration transmits a spectral range from 750 to 880 nm, yielding shaped 0.3 nJ pulses. After collinearly superimposing the shaper input with the orthogonally polarized reference beam, both are focused with a microscope objective ($60\times$; NA 0.7, MO1) onto a $50\ \mu\text{m}$ β -barium borate (BBO) (type II). The generated nonlinear signal, together with unconverted excitation light, is recollimated with a second microscope objective ($40\times$, NA 0.6, MO2). The desired sum-frequency signal can finally be extracted by a short-pass filter (Schott BG 42), and detected spectrally resolved in a CCD equipped spectrograph ($f=300$ mm). By not applying the GDD in the reference arm and introducing a variable delay Δt instead (shown as hatched beam path in Fig. 2), the setup can immediately be used as an independent *in situ* cross-frequency-resolved optical gating (XFROG) device,

where the unknown pulse is sampled by the 100 fs oscillator pulses and the resulting SFG spectrum is recorded for each Δt .

4. PREPARATIONS FOR SAC-SPIDER OPERATION

A. Creation of Pulse Doublets

In the present study, a spectrum with a bandwidth $\Delta\omega$ of 400 THz was used, which illuminated approximately $N=450$ pixels. According to Eq. (5), the maximum delay τ is therefore ~ 1.75 ps, which allows complete coverage of the usual double-pulse spacing range found in SPIDER literature. To verify the successful creation of pulse doublets, we have applied mask functions $\tilde{M}_{SLM}(\omega)$ for different delays τ and recorded *in situ* frequency resolved cross correlations. Details of the XFROG measurements are given in Section 6, where we use this technique to independently verify the SAC-SPIDER results. The experimental XFROG traces are shown in Fig. 3. In the top row [Fig. 3(a)], a cross correlation of the unshaped input pulse, which is to be characterized and compressed by SAC-SPIDER, can be seen. In this case, no mask function was applied to the shaper. The trace shown thus corresponds to the unknown pulse $E_{in}(t)$. Double pulses have been created with increasing temporal separations τ (200, 800, and 1600 fs). As can be seen in Fig. 3(b), for 200 fs, the resulting pulse is not a well-separated doublet, because the duration of $E_{in}(t)$ still exceeds τ . Therefore, the replicas of $E_{in}(t)$ overlap and yield an interference pattern in the XFROG trace. For $\tau=800$ fs, the pulses are clearly separated. It can be seen that each of the replicas, within the experimental noise of the XFROG implementation, exactly matches the unshaped $E_{in}(t)$. Even twice this temporal separation $\tau=1600$ fs allows the successful creation of double pulses with our pulse-shaping approach, as expected from the estimation based on Eq. (5).

B. Calibration Procedures

Apart from a carefully calibrated pulse shaper and spectrograph, there are three specific calibration steps that

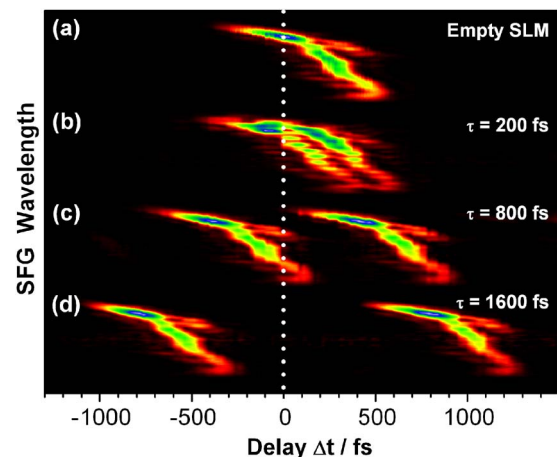


Fig. 3. (Color online) Experimental confirmation of the double-pulse shaping by frequency-resolved cross correlation (XFROG, for details see Section 6). Shown are data sets for an (a) unshaped pulse and doublets with (b) $\tau=200$, (c) 800, and (d) 1600 fs.

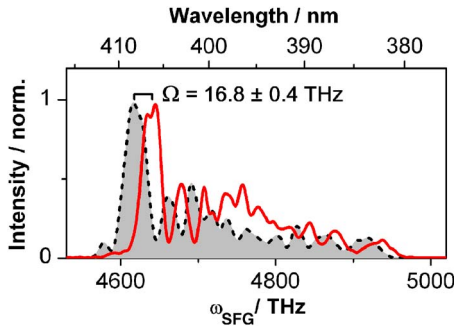


Fig. 4. (Color online) Calibration of the spectral shear with SAC-SPIDER. Shown are two spectra created by sum-frequency mixing of a single test pulse replica delayed by the shaper to 300 fs ($+\tau/2$, solid curve) and -300 fs ($-\tau/2$, dashed curve and shaded area), respectively, with the chirped reference pulse.

have to be performed for successful operation of SAC-SPIDER. First, the measured spectral phase $\phi(\omega)$ is going to be inverted and fed back to the pulse shaper. Therefore, the mapping between the fundamental frequency ω of the pulse to be characterized and the sum frequency $\omega_{\text{SFG}} = \omega + \omega_{\text{ref}}$, where ω_{ref} is the effective mixing frequency of the reference pulse, must be known. With the amplitude modulation capabilities of the pulse shaper, this relation can be very conveniently established, by simply creating a narrow spectral feature at frequency ω' in the supercontinuum and measuring this at a known frequency ω'_{SFG} in the sum-frequency spectrum.

The second calibration requirement is the determination of the spectral shear Ω for the given chirped reference pulse and the temporal separation τ of the test pulse replica. Again, with SAC-SPIDER, this can be achieved in a fully automatic scheme without any changes to the setup. Instead of creating a pulse doublet with a SLM mask function, the test pulse is only shifted in time by $\pm\tau/2$ using the pulse shaper. This is very easily achieved with a phase-only modulation, introducing the spectral phases $\phi_{\text{SLM}}(\omega) = \pm(\omega - \omega_0)\tau/2$ one after the other, and recording the respective sum-frequency spectrum of the delayed pulses. As the pulse at $-\tau/2$ overlaps with a different color of the chirped reference pulse than at $+\tau/2$, the spectral shift of the sum-frequency spectrum immediately gives the shear Ω . To exactly determine Ω , it is necessary to have easily distinguishable spectral features, such as the maximum of a smooth Gaussian spectrum or a sharp dip or peak. If the spectrum of the unknown pulse does not show such a suited spectral feature, the pulse shaper can always create one by amplitude modulation, making the determination of Ω with SAC-SPIDER very easy and straightforward.

An example of two spectra recorded by sum-frequency mixing of two test pulse replicas at $+\tau/2$ and $-\tau/2$ for $\tau = 600$ fs is shown in Fig. 4. The test pulse spectrum is well reproduced for both replicas, only showing some minor deviations in the relative intensities due to the mixing with different parts of the chirped reference pulse. Comparing distinct spectral features of the upconverted replicas, the spectral shear Ω is determined as the average of eight different positions yielding $\Omega = 16.8 \pm 0.4$ THz.

Finally, for the SPIDER measurement of the spectral phase, the temporal separation τ of the double pulses has

to be known precisely. As already stated in Subsection 2.A, the temporal delay between the interfering pulse doublet is directly proportional to the fundamental frequency of the interference fringes. In the SPIDER phase retrieval, the linear contribution of τ to the phase difference between the test pulse replicas has to be subtracted. As discussed in Subsection 2.A, an incorrect value of τ will, in the SPIDER algorithm, lead to an erroneous quadratic contribution in the recovered phase. Additionally, deviations in the spectrometer calibration are known to lead to systematic errors in the recovered phase.³¹ With a simple procedure, already applied in the seminal SPIDER work,¹⁷ these issues can be addressed: it is only necessary to record an interferogram of upconverted replica pulses that are delayed, but not spectrally sheared. Due to the fact that $\Omega=0$, the interferometric fringes only contain the linear phase term $\omega\tau$ and additional contributions due to residual errors of the spectrometer calibration. This phase difference can now be subtracted from any SPIDER measurement before the final integration step in the algorithm. To obtain the desired interferogram of upconverted, but spectrally not sheared replica, two approaches are viable with SAC-SPIDER. To begin with, due to the collinear nature of SAC-SPIDER, it is possible to simply rotate the nonlinear crystal in the microscope focus for type-I frequency mixing (both beams polarization parallel to the ordinary axis) and blocking the reference beam. Thereby, each of the delayed pulse replicas is frequency doubled yielding the desired interferogram with $\Omega=0$. Such calibration interferograms are shown in Fig. 5(a) for different values of τ . To obtain the wanted linear phase difference $\omega\tau$, the interferograms are processed in the SPIDER algorithm as described in Subsection 2.A, with-

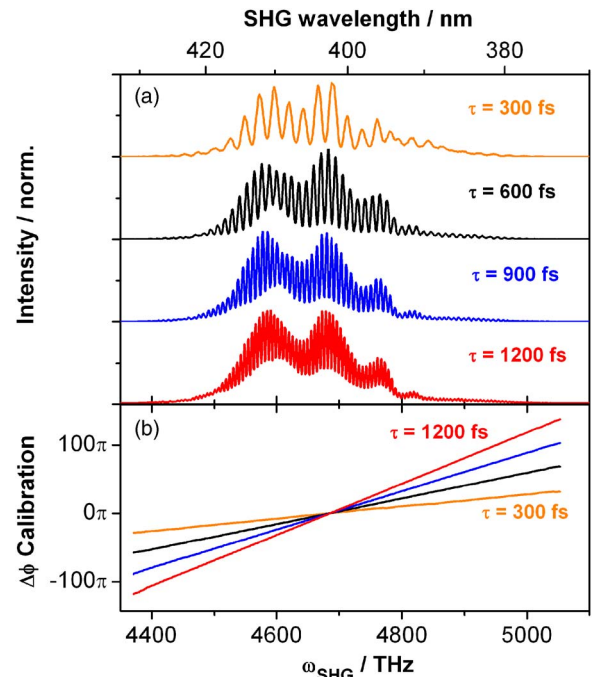


Fig. 5. (Color online) τ calibration. (a) SHG-calibration interferograms for different separations of the test pulse doublet. (b) Phase differences retrieved from the calibration interferograms corresponding to the linear term introduced by τ (see text for details).

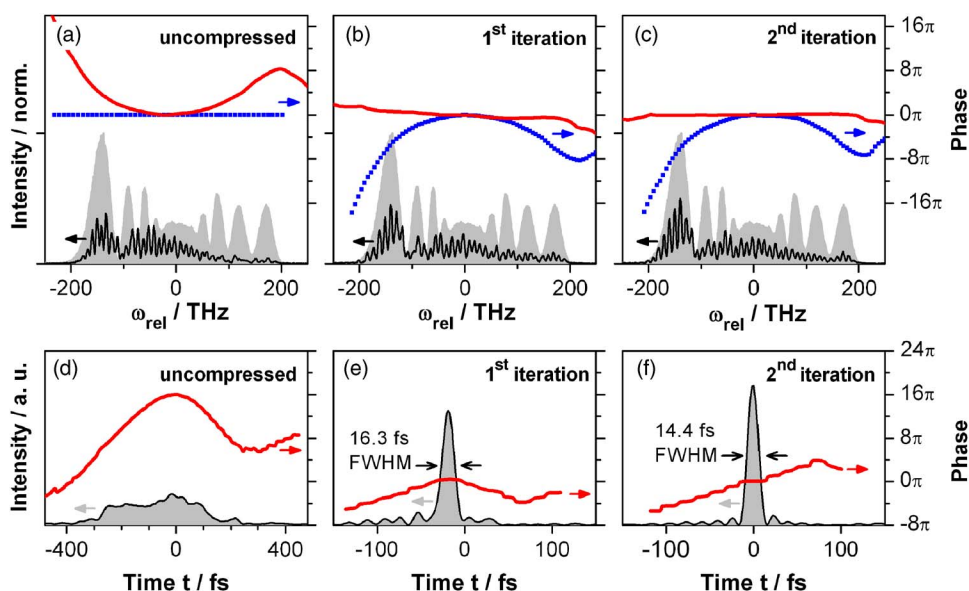


Fig. 6. (Color online) *In situ* pulse compression with SAC SPIDER. Shown are (a)–(c) the pulse spectra, interferograms, and phases in the frequency domain, and (d)–(f) reconstructed temporal pulse profiles and phases. From left to right, the compression sequence can be followed with (a) and (d) the uncompressed case, (b) and (e) the first, and (c) and (f) the second compression iteration. (a)–(c) The spectral phases are shown as thick solid curves, the shaper correction phase $\varphi_{corr}(\omega)$ as squares, interferograms as thin solid curves, and the fundamental pulse spectrum as the gray shaded area. All frequency domain data are shown relative to the pulse central frequency $\omega_{rel}=0$. (d)–(f) The temporal pulse intensity is shown as the gray shaded area with a thin contour, the temporal phase as a thick solid curve. Note that the uncompressed pulse in (d) and the compressed pulses in (e) and (f) are shown with different time scales for clarity.

out the last concatenation or integration step. This calibration phase is then stored in the SAC-SPIDER software, and subsequently subtracted prior to concatenation from any phase differences in SPIDER measurements with $\Omega \neq 0$. Note, that the mentioned deviations from a perfect linear phase difference $\omega\tau$ due to spectrometer errors are too small to be discernible in Fig. 5(b), except at the very edges of the second-harmonic generation (SHG) spectrum. However, they have to be taken into account and subtracted with the calibration procedure for a precise SPIDER phase measurement.

The SHG procedure described so far is carried out very easily, but can only be used if the second harmonic of the test pulses lies in the same frequency range as the sum-frequency of the test pulse mixed with the reference pulse, which is evaluated for the SPIDER measurement. Additionally, the intensity of the test pulses needs to be high enough to generate enough SHG signal to detect, because in this calibration step, they are not mixed with a strong reference beam. If this is not the case, a second approach can always be used, which is based on the same sum-frequency mixing process as the SAC-SPIDER measurement. In this approach, the chirped reference beam is filtered to a very narrow spectral portion, which corresponds to a long (picosecond) pulse with approximately constant frequency. Now, the test pulse doublet is mixed in the type-II nonlinear crystal, yielding two unconverted, but spectrally not shifted replicas with $\Omega=0$. In this procedure, the reference interferogram with $\Omega=0$ is always created in the same spectral position where the SPIDER measurement is being performed. Furthermore, a strong reference beam can be used if very weak test pulses are to be characterized. The spectral filtering can be achieved either by a very narrow interference bandpass filter in the reference beam, or conveniently by geometrical filtering

in the Fourier plane, if the chirp of the reference beam is introduced by a grating stretcher, as is the case in our experimental implementation. All the calibration steps can easily be completed within a few minutes, without changes to the experimental setup.

5. SAC-SPIDER OPERATION

A. *In situ* Phase Measurement and Pulse Compression

With the SAC-SPIDER apparatus carefully calibrated, it can immediately be used for *in situ* pulse compression. As already mentioned in the description of the experimental setup, the microscopic sample is replaced by a thin slab of a nonlinear crystal (BBO). Therefore, all dispersive elements including the focusing microscope objective are taken into account. It is easily possible to include coverslips and even immersion media, depending on the microscopic application. The unknown test pulse in this study is formed by supercontinuum generation in a PCF. Prior to compression, it is stretched in time over more than 450 fs at the site of the nonlinear interaction in the microscope, which can be estimated from the XFROG trace in Fig. 3(a). To characterize this pulse, the first step is to apply a double-pulse forming mask function $\tilde{M}_{SLM}(\omega)$ (see Subsection 2.B). The temporal spacing of the double pulse τ has to be chosen appropriately for the given bandwidth, to achieve a set of experimental parameters τ and Ω that fulfil the SPIDER requirements described in Subsection 2.A. Here, τ was chosen to be 600 fs, which gives a calibrated spectral shear of $\Omega=16.8 \pm 0.4$ THz. This value of Ω is well within the desired range for the bandwidth $\Delta\omega$ of 400 THz. The compression of the test pulse with these parameters is summarized in Fig. 6. Sum-frequency mixing of the test pulse doublet with the chirped reference beam

in the nonlinear crystal gives the SPIDER interferogram of the uncompressed pulse, as can be seen in Fig. 6(a) as a thin solid curve. Comparing the frequency-shifted interferogram with the independently measured spectrum of the test pulse [Fig. 6(a), gray shaded area] confirms that all frequency components are upconverted in the SFG process. From the interferogram, it can already be discerned that the fringe spacing is nonuniform. This corresponds to the spectral phase difference of the spectrally sheared test pulse replica being nonzero. Accordingly, the SPIDER algorithm retrieves a spectral phase [Fig. 6(a), thick solid curve] that is dominated by a quadratic term but also has complex higher-order contributions. This phase measurement is performed with the pulse shaper acting only as dispersionless interferometer, i.e., no additional phase $\varphi_{corr}(\omega)$ has been applied. $\varphi_{corr}(\omega)=0$ is depicted in Fig. 6(a) as squares.

The phase information obtained can now directly be used to apply a correction phase $\varphi_{corr}(\omega)$ in the pulse shaper. Evidently, the necessary correction phase is the sign-inverted measured phase of the unknown test pulse. This correction phase is shown in Fig. 6(b) as squares. By applying the modified mask function $\tilde{M}_{SLM}(\omega)$ containing the correction, the interferogram changes [Fig. 6(b), thin solid curve]. Accordingly, the reconstructed phase [Fig. 6(b), thick solid curve] is much more flat. Still, there are remaining undulations in the residual phase. This residue can, however, simply be added to $\varphi_{corr}(\omega)$ in an iterative manner. Thus, in the second iteration step [Fig. 6(c)] the interferogram only shows subtle changes. The retrieved phase is now almost perfectly flat, and compression is successfully achieved. This is confirmed when considering the reverse Fourier transform of the frequency domain data in the time domain to reconstruct the pulse shapes. The uncompressed test pulse [Fig. 6(d)] is stretched in time over more than 450 fs, as expected, and has a mainly quadratic temporal phase in the central part. The first compression step already produces a dramatic effect, as the pulse resulting from the flattened spectral phase has a temporal duration of only 16.3 fs (FWHM). The second iteration corrects for remaining phase distortions and results in a clean 14.4 fs (FWHM) pulse, which is very close (less than 4%) to the calculated Fourier limit of 13.9 fs (FWHM) for this spectrum.

In principle, the combination of SPIDER pulse characterization and pulse shaping is capable of noniterative pulse compression.³² The fact that here the first iteration is not yet giving the optimal compression result can have two reasons. First of all, the assumption that the instantaneous frequency remains constant during the length of the test pulse is not very well fulfilled at the beginning. Uncompressed pulses have several hundred femtosecond durations, while the chirped reference pulse ($\phi'' = 37,000 \text{ fs}^2$) has $\sim 1.5 \text{ ps}$. Such cases of highly chirped test pulses have very recently been thoroughly investigated,³³ and it was found that only a modified retrieval scheme taking into account a chirp-dependent shear will measure the correct phase, while the conventional approach based on the constant frequency assumption will generally underestimate the phase. This is the main reason for the remaining residual phase after the first SAC-SPIDER iteration seen in Fig. 5(b) as a thick solid curve. After this first

iteration, the pulse is short enough to perfectly fulfill the instantaneous frequency requirement; therefore the measured residual phase is correct and the compression succeeds with the second iteration. A second reason why iterations can be necessary in SAC-SPIDER is because of errors in the calibration of Ω . As the measured phase is proportional to Ω^{-1} , a too large shear will underestimate, while a too small Ω will overestimate the measured phase. Iteration, however, makes SAC-SPIDER very robust against even grossly deviating values of Ω . In fact, errors in the estimates of Ω only increase the number of iterations until the residual phase approaches zero. Based on that it becomes clear that Ω was determined precisely for the experiment in Fig. 6, as the first iteration already performs almost all of the compression.

B. Measurement Time and Retrieval of Complex Phases

The complete compression in Fig. 6 was performed very rapidly in less than 2 s. The phase measurement itself in SAC-SPIDER is only limited by the acquisition time of the CCD camera and the time needed to perform the SPIDER algorithm. This is a general property of SPIDER techniques and has already been demonstrated for real-time measurements.¹⁹ An iteration step for *in situ* compression takes a little bit longer, as now the limiting factor is the rate at which the pulse shaper can be updated. The unit used in this study is equipped with a rather slow serial computer interface, which limits the rate at which mask functions $\tilde{M}_{SLM}(\omega)$ can be written on the SLM. For the present configuration, run-time measurements determined that the complete cycle of a SAC-SPIDER measurement, phase inversion, and writing of the modified mask function is completed within 780 ms.

The presence of the pulse shaper allows us to easily evaluate the capabilities of the system to characterize pulses with even more complex pulse shapes. On the basis of the correction phase $\varphi_{corr}(\omega)$, which creates a clean pulse with a flat spectral phase, additional phase modulations $\varphi_{mod}(\omega)$ can be added. This means that the phase of the mask function $\varphi_{SLM}(\omega)$ now consists of the phase modulation necessary for the creation of double pulses, the correction phase $\varphi_{corr}(\omega)$ and $\varphi_{mod}(\omega)$. In Fig. 7, some

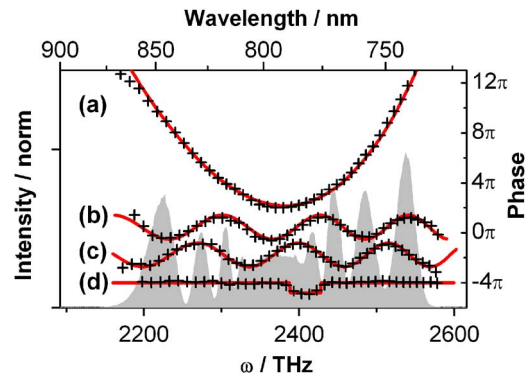


Fig. 7. (Color online) Retrieval of complex phases. In addition to the compressed pulse, arbitrary phase modulations $\varphi_{mod}(\omega)$ were applied: (a) quadratic phase with 2000 fs^2 , (b) and (c) sinusoidal phases with $\pi/2$ phase offset, (d) rectangular phase indentation. $\varphi_{mod}(\omega)$ is always shown as a thick solid curve, and the retrieved SAC-SPIDER phases as crosses. For comparison, the pulse spectrum is indicated as the gray shaded area.

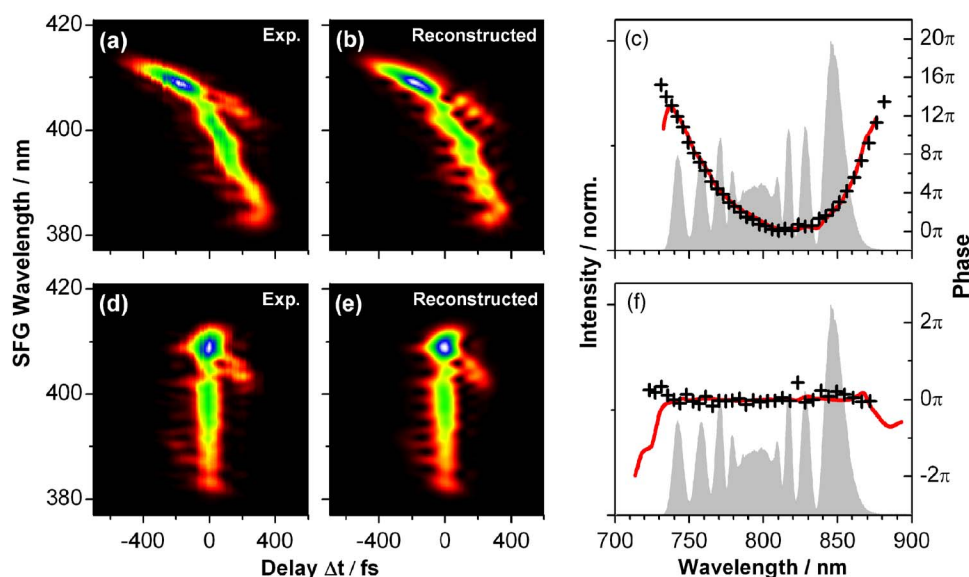


Fig. 8. (Color online) Comparison between SAC-SPIDER and XFROG methods. Both methods retrieved the same phase for (a)–(c) uncompressed and (d)–(f) the compressed supercontinuum pulses. The experimental XFROG traces [(a) and (d)] were reconstructed [(b) and (e)], respectively) and the spectral phase was retrieved [crosses in (c) and (f), respectively]. The corresponding phases measured with SAC-SPIDER are shown as solid lines and the test pulse spectrum is indicated as the gray shaded area. Note that the SAC-SPIDER phase shown in (c) is obtained after two iterations (compare Fig. 6).

examples for typical phase modulations $\varphi_{mod}(\omega)$ are shown, which are frequently used in coherent control.³⁴ In Fig. 7(a), an additional quadratic phase of $\varphi_{mod}(\omega) = 2000 \text{ fs}^2 (\omega - \omega_0)^2$ (solid curve) was added and successfully retrieved by the SAC-SPIDER (crosses). Similarly, sinusoidal phases of the type $\varphi_{mod}(\omega) = A \sin(\tau_m \omega + c)$ were added with amplitude $A = \pi$, modulation frequency $\tau_m = 50 \text{ fs}$, and a constant phase offset of $c = 0$ [Fig. 7(b)] and $c = \pi/2$ [Fig. 7(c)]. In both cases, the oscillating phase is nicely retrieved, and the phase shift between Figs. 7(b) and 7(c) is clearly discernible. Sinusoidal phases are highly relevant for applications in nonlinear microscopy, as they can be used for selective multiphoton imaging^{35,36} and for single-beam coherent anti-Stokes Raman scattering microscopy,^{37,38} which allows chemical contrast with a single broadband femtosecond laser and a pulse shaper. Finally, in Fig. 7(d), a phase indent with a “depth” of 0.7π is shown, which is also successfully characterized. Much larger indentation depths, however, can lead to disruptions in the interferograms, which cause the SPIDER algorithm to introduce systematic errors in the reconstructed phase.

Similarly, if the spectrum of the unknown pulse is very much structured and if the spectral intensity drops to zero, the SPIDER phase retrieval loses track of the fringe phase and encounters phase-cycle slip errors, which lead to artificially large linear spectral phases for the spectrum after such a problematic area in the interferogram. This property is common to all SPIDER implementations. SAC-SPIDER, however, allows, in some cases, mitigating phase-cycle slip problems: Due to the creation of the double pulses with the shaper, the relative offset phase between both replicas can be adjusted independently from their temporal separation. This permits very easy shifting of the interference fringes in the SAC-SPIDER interferogram, which can help to overcome problems in the phase reconstruction. If an interference fringe is placed where

there is a sharp dip in the test pulse spectrum, the phase cycle slip can be avoided at this spectral position. Thus, from a series of interferograms recorded with different offset phases, much more robust phase information can be obtained for highly structured pulses.

6. COMPARISON WITH INDEPENDENT XFROG MEASUREMENTS

To independently verify the phase obtained with the SAC-SPIDER, XFROG measurements^{39–41} were performed *in situ*. As the reference pulse, the 100 fs laser oscillator was used. For this purpose, in the SAC-SPIDER setup (Fig. 2, hatched beam path) the reference beam is not chirped as for SPIDER measurements, but can be delayed by Δt using a linear moving stage. Additionally, linear chirp of the reference pulse could be compensated by a pair of gratings. The sum-frequency mixing signal between this reference beam and the beam of the test pulses was detected in the same setup, as described in Section 3. The 100 fs oscillator as the reference pulse that has a much longer duration than the compressed test pulse has to be carefully characterized. This was performed with an *in situ* FROG measurement of the reference pulse under the same experimental conditions, i.e., taking into account all optical dispersive elements.

In Fig. 8, the characterization of the test pulse with the *in situ* XFROG and SAC-SPIDER methods is shown for the uncompressed [Figs. 8(a)–8(c)] and compressed [Figs. 8(d)–8(f)] supercontinuum phase. For both situations, the agreement between the methods is almost perfect: the uncompressed pulse shows a spectral phase with a strong quadratic phase and higher-order contributions, which is correctly identified by SAC-SPIDER [Fig. 8(c), solid curve] and XFROG [Fig. 8(c), crosses]. When the SAC-SPIDER is used to compress the pulse *in situ*, the XFROG also finds a flat spectral phase [Fig. 8(f), crosses] and con-

firms the successful compression. The fact that the reference pulse is not Fourier-transform-limited but has some degree of higher-order phase distortions can be seen in the experimental XFROG traces in Fig. 8: They are, to some extent, smeared out in time. Note that the precise knowledge of these distortions in the reference pulse nevertheless allows a very accurate reconstruction of the test pulse, as can be seen from the very close match of the experimental [Figs. 8(a) and 8(d)] and retrieved [Figs. 8(b) and 8(e)] XFROG traces. However, the procedure to obtain the test pulse phase *in situ* with XFROG is much more time consuming (approaching, including reconstruction, several tens of minutes) and complicated than the original SAC-SPIDER measurement (less than a second).

7. MULTIPHOTON MICROSCOPY APPLICATION EXAMPLE

As shown in the above sections, SAC-SPIDER is a very useful tool for rapid and precise *in situ* compression even of very complex pulses in a nonlinear microscope. To demonstrate how valuable this precise phase control is for multiphoton microscopy, we performed two-photon fluorescence microscopy using our PCF source, and compare images obtained without and with SAC-SPIDER compression. The sample was prepared with a diluted solution of 8 μm monodisperse melamine-formaldehyde-resin microparticles labeled with Rhodamine B (Kisker Biotech) in water, which was placed within a 2×4 mm recess incised in a 100 μm thick Teflon spacer on a microscope slide, and sealed with a coverslip. The sample was mounted on a XYZ-closed loop piezotranslation stage (PI Nanocube), which allows a maximum scanning range of 100 μm in each direction with nanometer resolution. Placing the focal volume exactly inside a microparticle, the two-photon fluorescence spectrum of the labeling dye Rhodamine B could be recorded: In Fig. 9(a), the respective spectra can be seen for uncompressed [solid line, hatched in dark gray

in Fig. 9(a), temporal profile Fig. 6(d)] and compressed pulses [dashed line, hatched in light gray in Fig. 9(a), for temporal profile see Fig. 6(f)]. The integrated intensity of the two-photon fluorescence obtained with compressed pulses is more than 1 order of magnitude larger than for uncompressed pulses. Using the integrated fluorescence signal intensity, imaging of the microparticles could be performed. For each pixel recorded with a step size of 600 nm in the *X* and *Y* directions, the shaper first applied an empty mask function for the uncompressed pulses, and then the SAC-SPIDER correction phase for the compressed pulses. In Figs. 9(b) and 9(c), both resulting images are shown on a common normalized intensity scale. As expected, the image obtained with SAC-SPIDER compression has a much higher contrast. Apart from the optimization of the signal level, SAC-SPIDER now immediately allows imprinting additional wanted phase functions [such as the sine modulations shown in Figs. 7(b) and 7(c)], to perform selective multiphoton fluorescence microscopy with shaped pulses.^{35,36}

8. CONCLUSIONS

The SAC-SPIDER method permits full *in situ* phase measurement and control of broadband pulses in the environment of microscopy and microspectroscopy. We have discussed in detail the implementation of this new, to the best of our knowledge, simplified dispersion-free phase characterization method. As an example, we have shown the compression of a broadband supercontinuum from a photonic crystal fiber down to 14.4 fs, and we applied it for the improved multiphoton microscopic imaging of fluorescent microspheres. Successful compression and phase measurement has been verified by comparison with *in situ* XFROG traces. The key feature of SAC-SPIDER is the use of a femtosecond pulse shaper, which completely eliminates the need for an interferometer setup and, at the same time, introduces the possibility to compress complex pulses. The versatility and its straightforward implementation make SAC-SPIDER an extremely useful tool for next-generation broadband nonlinear microscopy, and for microspectroscopy, which can very much profit from precisely tailored femtosecond pulses incorporating coherent control schemes.

ACKNOWLEDGMENTS

Generous support by K.-L. Kompa and the Max-Planck Society, as well as a scholarship from the Fonds der Chemischen Industrie to B. von Vacano, are gratefully appreciated. The authors thank W. Wohlleben for stimulating discussions at the beginning of this project and J. Hauer for his valuable comments. M. Motzkus's e-mail address is motzkus@staff.uni-marburg.de.

REFERENCES AND NOTES

1. W. R. Zipfel, R. M. Williams, and W. W. Webb, "Nonlinear magic: multiphoton microscopy in the biosciences," *Nat. Biotechnol.* **21**, 1369–1377 (2003).
2. J. Squier and M. Muller, "High resolution nonlinear microscopy: a review of sources and methods for achieving optimal imaging," *Rev. Sci. Instrum.* **72**, 2855–2867 (2001).

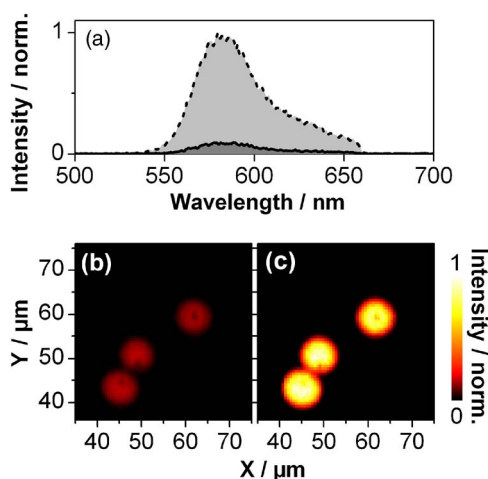


Fig. 9. (Color online) Application example of SAC-SPIDER compressed pulses in two-photon fluorescence microscopy. (a) Two-photon fluorescence spectra measured in a Rhodamine B labeled polymer particle with uncompressed (solid curve, hatched in dark gray) and compressed (dashed curve, hatched in light gray) pulses. Imaging of fluorescent microparticles with (b) uncompressed and (c) compressed pulses. The integrated fluorescence intensity is normalized on the same scale.

3. G. J. Brakenhoff, M. Muller, and J. Squier, "Femtosecond pulse width control in microscopy by two-photon absorption autocorrelation," *J. Microsc.* **179**, 253–260 (1995).
4. C. Soeller and M. B. Cannell, "Construction of a two-photon microscope and optimisation of illumination pulse duration," *Pfluegers Arch.* **432**, 555–561 (1996).
5. R. Wolleschensky, T. Feurer, R. Sauerbrey, and U. Simon, "Characterization and optimization of a laser-scanning microscope in the femtosecond regime," *Appl. Phys. B* **67**, 87–94 (1998).
6. M. Muller, J. Squier, R. Wolleschensky, U. Simon, and G. J. Brakenhoff, "Dispersion precompensation of 15 femtosecond optical pulses for high-numerical-aperture objectives," *J. Microsc.* **191**, 141–150 (1998).
7. A. M. Weiner, "Femtosecond pulse shaping using spatial light modulators," *Rev. Sci. Instrum.* **71**, 1929–1960 (2000).
8. D. Yelin, D. Meshulach, and Y. Silberberg, "Adaptive femtosecond pulse compression," *Opt. Lett.* **22**, 1793–1795 (1997).
9. T. Baumert, T. Brixner, V. Seyfried, M. Strehle, and G. Gerber, "Femtosecond pulse shaping by an evolutionary algorithm with feedback," *Appl. Phys. B* **65**, 779–782 (1997).
10. D. Zeidler, S. Frey, K. L. Kompa, and M. Motzkus, "Evolutionary algorithms and their application to optimal control studies," *Phys. Rev. A* **64**, 023420 (2001).
11. D. N. Fittinghoff, J. A. Squier, C. P. J. Barty, J. N. Sweetser, R. Trebino, and M. Muller, "Collinear type II second-harmonic-generation frequency-resolved optical gating for use with high-numerical-aperture objectives," *Opt. Lett.* **23**, 1046–1048 (1998).
12. I. Amat-Roldan, I. G. Cormack, P. Loza-Alvarez, E. J. Gualda, and D. Artigas, "Ultrashort pulse characterisation with SHG collinear-FROG," *Opt. Express* **12**, 1169–1178 (2004).
13. I. Amat-Roldan, I. G. Cormack, P. Loza-Alvarez, and D. Artigas, "Starch-based second-harmonic-generated collinear frequency-resolved optical gating pulse characterization at the focal plane of a high-numerical-aperture lens," *Opt. Lett.* **29**, 2282–2284 (2004).
14. A. Monmayrant, M. Joffre, T. Oksenhendler, R. Herzog, D. Kaplan, and P. Tournois, "Time-domain interferometry for direct electric-field reconstruction by use of an acousto-optic programmable filter and a two-photon detector," *Opt. Lett.* **28**, 278–280 (2003).
15. V. V. Lozovoy, I. Pastirk, and M. Dantus, "Multiphoton intrapulse interference. IV. Ultrashort laser pulse spectral phase characterization and compensation," *Opt. Lett.* **29**, 775–777 (2004).
16. B. Xu, J. M. Gunn, J. M. Dela Cruz, V. V. Lozovoy, and M. Dantus, "Quantitative investigation of the multiphoton intrapulse interference phase scan method for simultaneous phase measurement and compensation of femtosecond laser pulses," *J. Opt. Soc. Am. B* **23**, 750–759 (2006).
17. C. Iaconis and I. A. Walmsley, "Spectral phase interferometry for direct electric-field reconstruction of ultrashort optical pulses," *Opt. Lett.* **23**, 792–794 (1998).
18. C. Iaconis and I. A. Walmsley, "Self-referencing spectral interferometry for measuring ultrashort optical pulses," *IEEE J. Quantum Electron.* **35**, 501–509 (1999).
19. T. M. Shuman, M. E. Anderson, J. Bromage, C. Iaconis, L. Waxer, and I. A. Walmsley, "Real-time SPIDER: ultrashort pulse characterization at 20 Hz," *Opt. Express* **5**, 134–143 (1999).
20. B. von Vacano, T. Buckup, and M. Motzkus, "In situ broadband pulse compression for multiphoton microscopy using a shaper-assisted collinear SPIDER," *Opt. Lett.* **31**, 1154–1156 (2006).
21. M. Takeda, H. Ina, and S. Kobayashi, "Fourier-transform method of fringe-pattern analysis for computer-based tomography and interferometry," *J. Opt. Soc. Am.* **72**, 156–160 (1982).
22. P. Baum, S. Lochbrunner, and E. Riedle, "Zero-additional-phase SPIDER: full characterization of visible and sub-20-fs ultraviolet pulses," *Opt. Lett.* **29**, 210–212 (2004).
23. M. E. Anderson, L. E. E. de Araujo, E. M. Kosik, and I. A. Walmsley, "The effects of noise on ultrashort-optical-pulse measurement using SPIDER," *Appl. Phys. B* **70**, S85–S93 (2000).
24. E. M. Kosik, A. S. Radunsky, I. A. Walmsley, and C. Dorrer, "Interferometric technique for measuring broadband ultrashort pulses at the sampling limit," *Opt. Lett.* **30**, 326–328 (2005).
25. J. R. Birge, R. Ell, and F. X. Kartner, "Two-dimensional spectral shearing interferometry for few-cycle pulse characterization," *Opt. Lett.* **31**, 2063–2065 (2006).
26. L. Gallmann, D. H. Sutter, N. Matuschek, G. Steinmeyer, and U. Keller, "Techniques for the characterization of sub-10-fs optical pulses: a comparison," *Appl. Phys. B* **70**, S67–S75 (2000).
27. H. Rabitz, R. de Vivie-Riedle, M. Motzkus, and K.-L. Kompa, "Whither the future of controlling quantum phenomena?," *Science* **288**, 824–828 (2000).
28. W. Wohlleben, T. Buckup, J. L. Herek, and M. Motzkus, "Coherent control for spectroscopy and manipulation of biological dynamics," *ChemPhysChem* **6**, 850–857 (2005).
29. D. N. Fittinghoff, A. C. Millard, J. A. Squier, and M. Muller, "Frequency-resolved optical gating measurement of ultrashort pulses passing through a high numerical aperture objective," *IEEE J. Quantum Electron.* **35**, 479–486 (1999).
30. A 3:1 beam splitter was chosen to generate the reference beam to maintain a sufficient power level for the creation of the desired supercontinuum spectrum. An optimal choice might be different for other applications; in our case it ensures high-enough pulse energies of the compressed test pulses *in situ* for microscopy.
31. C. Dorrer, "Influence of the calibration of the detector on spectral interferometry," *J. Opt. Soc. Am. B* **16**, 1160–1168 (1999).
32. J. Thornes, P. Poon, and M. E. Anderson, "Single-iteration compression of femtosecond laser pulses," *J. Opt. Soc. Am. B* **21**, 1387–1390 (2004).
33. J. Wemans, G. Figueira, N. Lopes, and L. Cardoso, "Self-referencing spectral phase interferometry for direct electric-field reconstruction with chirped pulses," *Opt. Lett.* **31**, 2217–2219 (2006).
34. T. Hornung, R. Meier, and M. Motzkus, "Optimal control of molecular states in a learning loop with a parameterization in frequency and time domain," *Chem. Phys. Lett.* **326**, 445–453 (2000).
35. J. M. Dela Cruz, I. Pastirk, V. V. Lozovoy, K. A. Walowicz, and M. Dantus, "Multiphoton intrapulse interference 3: probing microscopic chemical environments," *J. Phys. Chem. A* **108**, 53–58 (2004).
36. J. P. Ogilvie, D. Debarre, X. Solinas, J. L. Martin, E. Beaurepaire, and M. Joffre, "Use of coherent control for selective two-photon fluorescence microscopy in live organisms," *Opt. Express* **14**, 759–766 (2006).
37. N. Dudovich, D. Oron, and Y. Silberberg, "Single-pulse coherently controlled nonlinear Raman spectroscopy and microscopy," *Nature* **418**, 512–514 (2002).
38. B. von Vacano, W. Wohlleben, and M. Motzkus, "Actively shaped supercontinuum from a photonic crystal fiber for nonlinear coherent microspectroscopy," *Opt. Lett.* **31**, 413–415 (2006).
39. X. Gu, L. Xu, M. Kimmel, E. Zeek, P. O'Shea, A. P. Shreenath, R. Trebino, and R. S. Windeler, "Frequency-resolved optical gating and single-shot spectral measurements reveal fine structure in microstructure-fiber continuum," *Opt. Lett.* **27**, 1174–1176 (2002).
40. S. Linden, H. Giessen, and J. Kuhl, "XFROG—a new method for amplitude and phase characterization of weak ultrashort pulses," *Phys. Status Solidi B* **206**, 119–124 (1998).
41. S. Linden, J. Kuhl, and H. Giessen, "Amplitude and phase characterization of weak blue ultrashort pulses by downconversion," *Opt. Lett.* **24**, 569–571 (1999).